34th EPS Conference on Plasma Phys. Warsaw, 2 - 6 July 2007 ECA Vol.31F, P-1.023 (2007)

Plasma-wall heat loads in ITER-like advanced Tokamak scenarios on JET

G. Arnoux[1], P. Andrew[2], M. Beurskens[2], S. Brezinsek[3], C. Challis[2], P. De Vries[2], W. Fundamenski[2], E. Gauthier[1], C. Giroud[2], A. Huber[3], S. Jachmich[4], X. Litaudon[1], R.A. Pitts[5], F. Rimini[1] and JET EFDA contributors*

[1] *Association EURATOM-CEA, DSM/DRFC, CEA/Cadarache, F-13108 St Paul-Lez-Durance, France*

[2] *EURATOM/UKAEA Fusion Association, Culham Science Center, Abingdon, Oxon, OX14 3DB, UK*

[3] *Institut für Energieforschung - Plasmaphysik, Forschungzentrum Jülich, Trilateral Euregio Cluster, EURATOM-Assoziation, D-52425 Jülich, Germany*

[4] *Association "EURATOM-Belgian State" Laboratory for Plasma Physics Koninklijke Militaire scholl - Ecole Royale Militaire Renaissancelaan 30 Avenue de la renaissance, B-1000 Brussels Belgium.*

[5] *Association EURATOM-Confédération Suisse, Ecole Polytechnique Fédérale de Lausanne (EPFL), CRPP, CH-1015 Lausanne, Switzerland*

Introduction

Advanced tokamak (AT) scenarios have been developed with the aim of steady-state operation [1]. They operate at relatively low densities (central line average density: $n_{e,av} \leq 4 \cdot 10^{19}$ m^{-3} on JET) and high additional power (20MW $\leq P_{add} \leq$ 30MW on JET), both of which necessary to ensure a large fraction of non inductive current. This leads to hot edge plasmas ($20 \leq T_e \leq 30eV$ at the targets on JET) and hence low recycling condition with partial divertor detachment difficult, if not impossible to achieve. The power handling capability of the plasma-facing components (PFC) during AT scenarios is a key issue [2] regarding the next planned JET enhancements: P_{add} increased to 45MW with duration up to 20s, and the ITER-like wall project: beryllium PFCs for the main chamber and a tungsten divertor [3].

Here, for the first time on JET an attempt has been made to characterise the edge plasma of AT scenarios in an ITER-like configuration. New AT scenarios have been developed to investigate their compatibility with plasma-wall interactions. In particular impurity injection techniques have been developed for two reasons: the reduction of the continuous heat load on the divertor target by increasing the radiated fraction and cooling dawn the divertor plasma, which is discussed in the present paper, and the ELM mitigation in order to reduce their penetration in the core plasma and avoid the destruction of the internal transport barrier (ITB), which is discussed in [4]. Impurity injection techniques have also been studied on JET in hybrid scenarios with type-III ELMs [5].

Experiments and results

The reference plasma discharge (ITER-AT) is a high triangularity configuration (Figure 1a) with $B_0 = 3.1$T, $I_p = 1.9$MA, $q_{95} \simeq 5.0$, $\delta = 0.42$, and with 24MW of additional power applied for 6s (144MJ total input energy). About 100MJ ($P_{rad}/P_{tot} \simeq 30\%$) is conducted to the PFCs of which 80% arrives at the divertor (from thermocouple measurements) and at

*See Appendix in M.L. Watkins et al., 21st IAEA Fusion Energy Conference, 2006, Chengdu, China

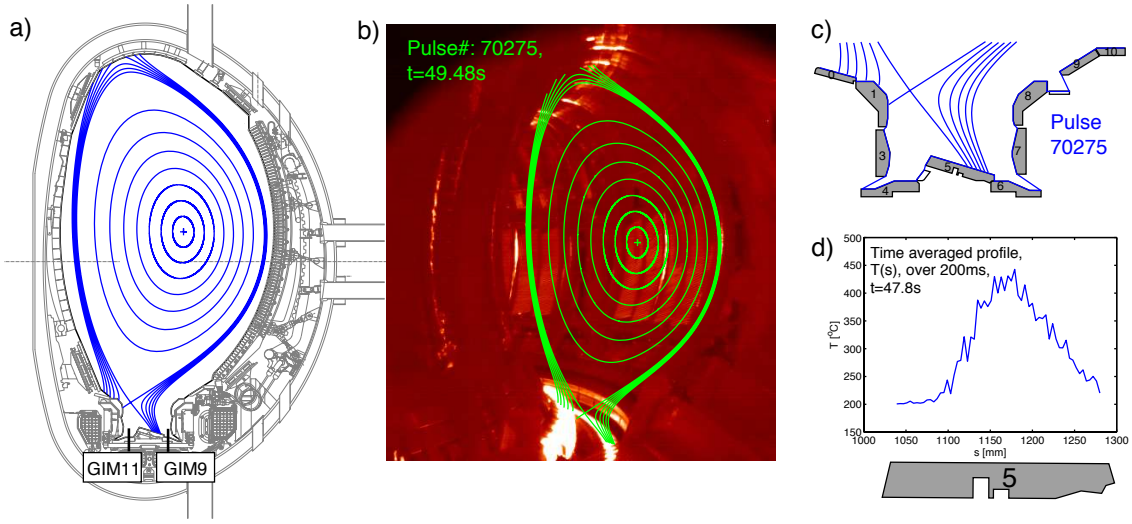

Figure 1: (a) Schematic view of the JET cross-section and the ITER-AT configuration (constant magnetic flux surfaces calculated with EFIT). Two gas injection locations, in the divertor SOL and in the private flux region are labelled GIM9 and GIM11 respectively. (b) Infrared image taken with the JET-EP wide angle IR camera (KL7) with superimposed flux surfaces. (c) Cross-section of the JET divertor with numbered tiles. The spacing of the SOL magnetic flux surfaces corresponds to 5mm mapped at the outer midplane radius. (d) Example of an IR temperature profile on the outer target after toroidal averaging (symmetry) at t=47.8s.

least 10% is conducted to the upper dump plate (from the IR measurement). Figure 1b is an IR image of the JET in-vessel PFCs where the white areas denote the hottest elements. This illustrates that the main plasma-wall interaction is on the divertor and the upper dump plate. The bright spots localised on the septums of the outer wall are interactions induced by RF heating (ICRH) [6] The plasma interaction with other outer limiters is negligible in the present configuration because the plasma-wall gap at the outer midplane is about 10cm when the scrape-off layer (SOL) e-folding length determined from the IR heat load profile (cf Figure 2f) is $\lambda_{SOL} \simeq 1.3$cm. The present paper focuses its study on the divertor inner and outer target heat load measurement using the JET-EP wide angle IR camera [7].

The IR heat load profiles, $q_{IR}(s,t)$, s being the length along the surface of the poloidal cross-section of the tile (Figure 2e and 2f), are calculated from the temperature profiles (toroidal averaging of the target surface temperature, see example in Figure 1d) using the 2D non-linear code THEODOR [9]. The tiles are modelled with a rectangle cross-sections and the effect of the carbon layer on the surface [10] is taken into account in the calculation assuming a uniform layer characterised by a heat transmission coefficient, α_{sl} (no heat capacity) [11]. The heat flux through the layer is such that: $q = \alpha_{sl} \cdot (T_{surf} - T_{bulk})$, where T_{bulk} is the tile surface temperature and T_{surf} is the surface layer temperature seen by the IR camera. In the present configuration, tile 5 is a net erosion area (no layer): $\alpha_{sl,outer} = 200 kW/m^2K$, whereas the horizontal part of tile 1, where the peak heat load is measured (Figure 2e), is a deposition area: $\alpha_{sl,inner} = 5 kW/m^2K$.

Figure 2 illustrates two typical scenarios, one with and one without impurity injection. It shows that impurity injection reduces the outer target peak temperature (Figure 2c), thus the peak heat load (Figure 2d). The scenario has been repeated for different gas injection locations (GIM9 and GIM11, see Figure 1a), gas species (Neon and Nitrogen) and

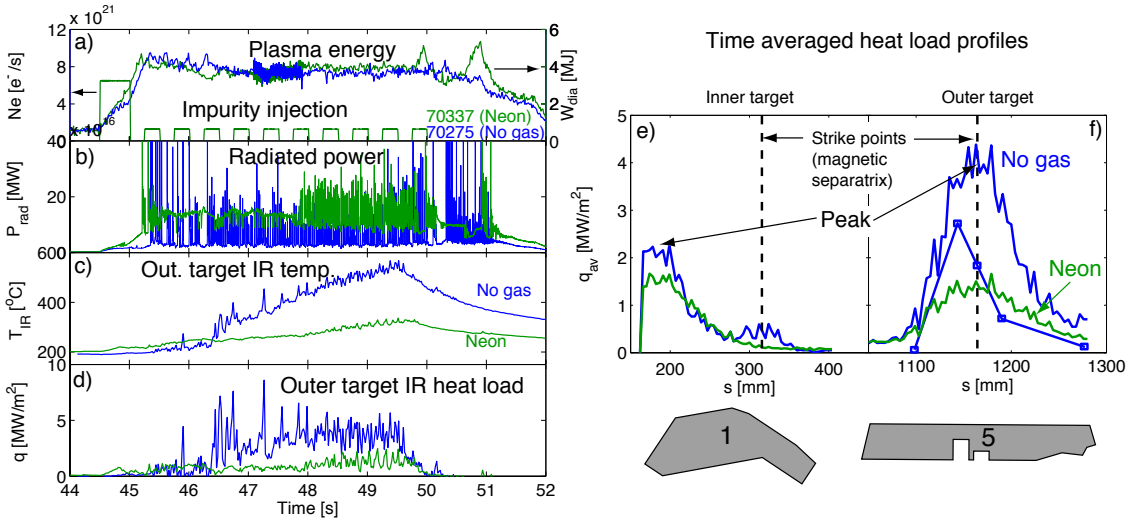

Figure 2: Two typical discharges without (70275) and with (70337) impurity injections. (a) Impurity injection wave form and plasma energy from the diamagnetic flux measurements. (b) Total radiated power. (c) Outer target IR peak surface temperature. (d) Outer target IR peak heat load. (e) and (f) Time averaged (on [47.5;49.5]s for pulse 70275 and [48.6;48.8]s for pulse 70337) IR heat load profiles for inner and outer target respectively. The outer target profile is compared with the heat load determined from the Langmuir probe measurements (squares) [8].

amount of gas. The total radiative power, P_{rad} (Figure 2b), is controlled using feed forward impurity injection (see wave-form in Figure 2a). Despite a constant fraction of radiated power (ELM averaged) during the discharge, the L to H-mode transition is difficult to control and the ELM behaviour can change during the discharge ($20 \leq f_{elm} \leq 220$Hz [4]). For the divertor heat load study, a 200ms time window is selected for both L and H mode phases between 47s and 49s where the strike point positions are fixed. To compare the effect of different radiative fraction level, P_{rad}/P_{tot}, one determine the peak heat loads, $q_{av,inner}$ and $q_{av,outer}$, of the inner and outer targets respectively from the time averaged profiles. As shown in Figure 2e and 2f the peak heat load coincides with the strike point position on tile 5 whereas on tile 1 the peak heat load is located on the horizontal part of the tile. The complex geometry of tile 1 combined with the variation of the pitch angle of the magnetic field lines along the tile make the interpretation of the heat load profile difficult. In the present work, $q_{av,inner}$, is taken at the maximum of the profile and not at the strike point position.

Figure 3 shows that $q_{av,outer}$ decreases by up to a factor 8 when $P_{rad}/P_{tot} \geq 50\%$ and this does not depend on the gas injection location or injected species whereas $q_{av,inner}$ is not significantly affected. In the ITER-AT configuration, the inner target heat load is difficult to decrease because the distance between the X-point and the target (about 10cm) is too short for the power to be dissipated by volumetric processes. In addition, the open divertor configuration leads to a low recycling regime. At high radiative fraction ($P_{rad}/P_{tot} \geq 50\%$) one find that $q_{av,outer}/q_{av,inner} < 1$ tough this number is to be taken cautiously. If the relative values of the heat load from tile to tile are reliable, the absolute value, hence the comparison between two tiles is more difficult because of the uncertainty due to the calculation. One find that on the tile 5 the accumulated energy calculated from the time and space integration of $q_{IR}(s,t)$, $E_{5,IR}$, is such that $E_{5,IR}/E_{5,TC} = 50-70\%$ where

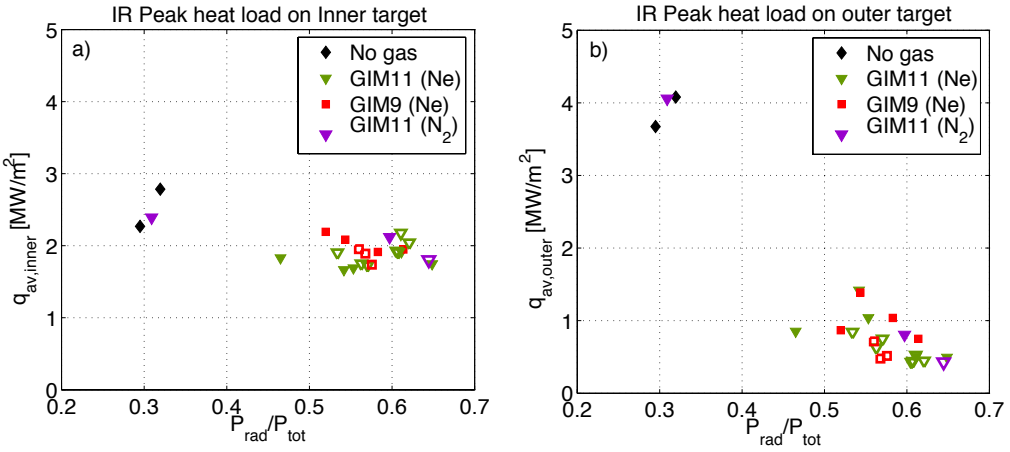

Figure 3: Peak heat load as a function of the fraction of radiated power (a) on the inner and (b) on the outer target calculated from IR thermography. The impurities ares injected in the private flux region (triangles) or in the SOL (squares) and lead to either H-mode (solid symbols) or L-mode (open symbols). Diamonds indicate reference pulses with no impurity injection.

$E_{5,TC}$ is determined from the thermocouple measurements. This is not systematic and it is planned to investigate this discrepancy more in detailed in the future. On tile 1 the discrepancy is rather $E_{1,IR}/E_{1,TC} = 75 - 90\%$. However the shape of tile 1 cross-section suggests that a rectangle cross-section model is probably not appropriate.

Conclusion

The present work provides the first characterisation of the divertor heat load using IR thermography during advanced tokamak scenarios in ITER-like cofiguration on JET. In future operation (power upgrade, ITER-like wall), divertor heat load might be challenging on the inner target, whereas on the outer target it can be significantly reduced using Neon or Nitrogen injection techniques. The gas species and gas injection location are not determinant parameters for the heat load reduction.

References

[1] A.A. Tuccillo et. al. *Nucl. Fusion*, 46, 2006.

[2] X. Litaudon et. al. *Proc. in this conference*, 2007.

[3] J. Pamela et. al. *J. Nucl. Mater.*, 363-365:1–11, 2006.

[4] M. Beurskens et. al. *Proc. in this conference*, 2007.

[5] Y. Corre et. al. *Proc. in this conference*, 2007.

[6] L. Colas et. al. *Proc. in this conference*, 2007.

[7] E. Gauthier et. al. *Proc. in 24th Symposium on Fusion Technology, Warsaw, Poland*, 2006.

[8] S. Jachmich et. al. *Proc. in this conference*, 2007.

[9] A. Herrmann et. al. *Plasma Phys.Control. Fusion*, 37:17–29, 1995.

[10] P. Andrew et. al. *J. Nucl. Mater.*, 313-316:135–139, 2003.

[11] T. Eich et. al. *Plasma Phys. Control. Fusion*, 49:573–604, 2007.